

## Optical Transitions in Quantum Wires with Strain-Induced Lateral Confinement

D. Gershoni, J. S. Weiner, S. N. G. Chu, G. A. Baraff, J. M. Vandenberg, L. N. Pfeiffer, K. West, R. A. Logan, and T. Tanbun-Ek

*AT&T Bell Laboratories, Murray Hill, New Jersey 07974*

(Received 23 February 1990)

Nanometer-scale quantum wires have been directly produced using an epitaxial-growth technique. Modulation of the in-plane lattice constant of a GaAs/GaAlAs quantum well, grown over an InGaAs/GaAs strained-layer superlattice, laterally confines the carriers to one dimension. These novel structures are studied by luminescence and luminescence-excitation spectroscopies and by transmission electron microscopy. Large energy shifts and polarization anisotropy are observed. The results compare very well with a theoretical model based on the effective-mass approximation and elastic and phenomenological deformation-potential theories.

PACS numbers: 73.20.Dx, 78.60.Hk, 78.65.Fa

Interest in structures having quantum confinement in more than one dimension arises both for their potential in uncovering new phenomena in condensed-matter physics and for their potential device applications.<sup>1</sup> Most of the reports to date involve fabrication of such structures by methods such as electron-beam lithography,<sup>2-6</sup> combined with impurity-induced interdiffusion,<sup>7</sup> stressor patterning,<sup>8</sup> or overgrowth of previously etched patterns.<sup>9</sup> Changes in the optical properties due to lateral confinement, such as blueshift of the luminescence and splitting of the subbands, have already been reported.<sup>4-6</sup> The lateral dimensions in these structures, however, have been much larger than the vertical dimensions obtained by epitaxial growth. Recently, two-dimensional band-gap modulation has been demonstrated by means of epitaxial growth on tilted superlattices<sup>10</sup> and by vapor levitation epitaxy.<sup>11</sup> These techniques seem to allow for lateral dimensions as small as the vertical one and overcome the damage creation associated with the previous techniques. They suffer, however, from nonuniformity and lack of control over the density, dimensions, and direction of the wires produced.

In this Letter we report on the investigations of the smallest quantum wires ever made. The structures were directly produced by epitaxial-growth techniques which allow for better control over the lateral dimension. Lateral confinement in our structures is achieved by strain-induced modulation of the in-plane lattice constant of a quantum well (QW).

The samples were prepared by two stages of epitaxial growth as schematically shown in Fig. 1(a). In the first stage, a 150-period InGaAs/GaAs strained-layer superlattice (SLS) was grown on a (001)-oriented GaAs substrate in an atmospheric-pressure metal-organic vapor-phase-epitaxial (MOVPE) system. Each period of the SLS contains 71 Å of In<sub>0.063</sub>Ga<sub>0.937</sub>As and 240 Å of GaAs. The SLS region was preceded by a 0.5- $\mu$ m-thick GaAs buffer layer and was capped with a  $\sim$ 3- $\mu$ m-thick GaAs layer. The dimensions, composition, and quality of the SLS were studied using cross-section transmission electron microscopy (TEM), high-resolution x-ray diffraction (HRXRD), and photoluminescence (PL).<sup>13</sup>

Misfit dislocations are observed only in the first interface between the buffer layer and the SLS. From their low density and from the HRXRD we conclude that the amount of strain relaxation in the SLS is negligible.

In the second stage of growth the samples were inserted into a molecular-beam-epitaxy machine. They were then cleaved *in situ* and the following sequence of layers was grown on the (110) cleaved facet: a 16-Å GaAs buffer layer, a 200-Å Al<sub>0.3</sub>Ga<sub>0.7</sub>As barrier, an 80-Å GaAs QW, a 200-Å Al<sub>0.3</sub>Ga<sub>0.7</sub>As barrier, a 34-Å GaAs QW, a 200-Å barrier, and a 50-Å GaAs cap layer. The calculated electronic potential for the 80-Å QW grown over one period of InGaAs strained layer is shown in Fig. 1(b). Figure 1(c) shows a dark-field TEM micrograph of the cross-sectional view of the sample using (00 $\bar{2}$ )

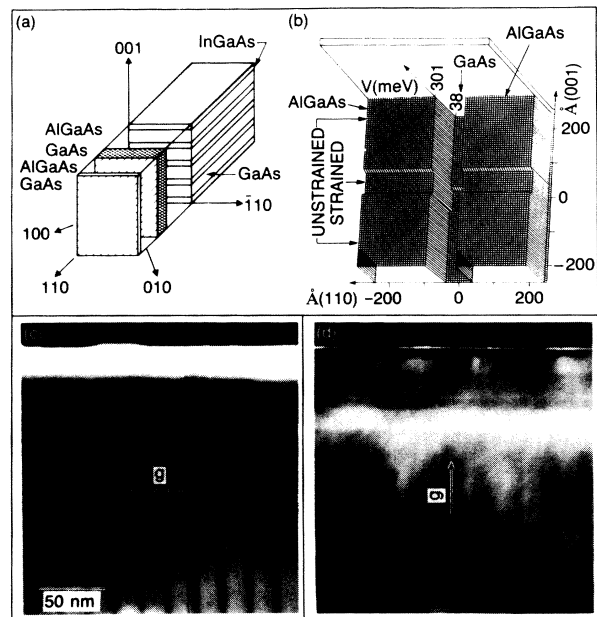


FIG. 1. (a) Schematic of the structure. (b) Calculated conduction-band potential for the 80-Å $\times$ 71-Å strained quantum wire. (c) (00 $\bar{2}$ ) and (d) (220) dark-field reflection TEM micrographs of the (110) side-grown quantum wires.

reflection. A high-quality, dislocation-free SLS is evident. Since the sample in Fig. 1(c) is tilted away from the  $(\bar{1}10)$  zone axis, the GaAs/AlGaAs QWs grown on the  $(110)$  cleavage plane do not show clear contrast. In Fig. 1(d) the  $(220)$  reflection is used. Here the QWs are more prominent and the SLS loses contrast. It is clear from the micrograph that the two QWs are of high quality and that they form a perfect crystallographic structure with the SLS beneath them. The lattice-constant modulation associated with the InGaAs/GaAs SLS is therefore expected to be uniform throughout the entire AlGaAs/GaAs QW structure. The unique ability to grow QWs on a cleaved  $(110)$  surface, which is essential for this study, is described elsewhere.<sup>14</sup>

Figure 2 displays low-temperature cathodoluminescence (CL), PL, and PL excitation (PLE) spectra of the sample. The spectra in Fig. 2(a) were obtained from QWs grown over the unstrained, cleaved GaAs substrate. Those in Fig. 2(b) were obtained from QWs grown over the SLS. The CL spectra (lowest curve, solid line) were obtained at 19 K using a 10-pA, 5-kV electron beam incident normal to the  $(110)$  plane. Using fixed-wavelength CL images, we have spatially resolved the different regions of the sample, verifying the source of each spectral feature. Three important points can be readily learned from the CL spectra. First, the luminescence peaks of the strained quantum wires (SQWR) associated with both the 80- and 34-Å QWs are shifted

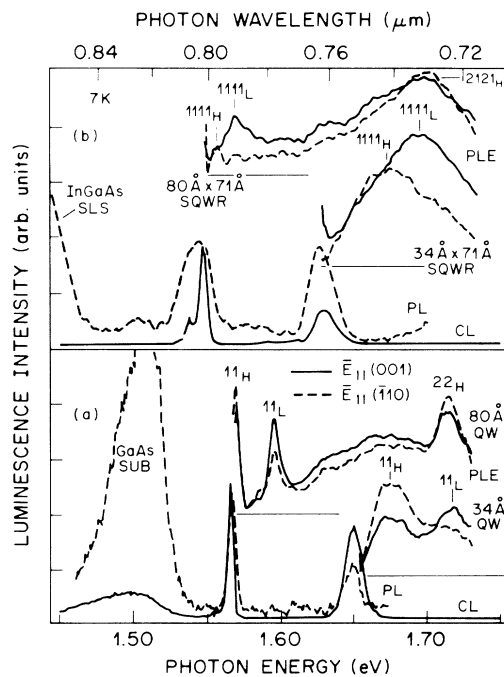


FIG. 2. Cathodoluminescence (CL), photoluminescence (PL), and PL excitation (PLE) spectra of (a)  $(110)$  side-grown quantum wells and (b)  $(110)$  side-grown strained quantum wires. The PLE spectra are shifted vertically for clarity, and the zeros are indicated by horizontal lines.

$\sim 21$  meV to the red relative to the unstrained QWs. The uniform shift indicates that both QWs experience the same strain though they are spatially separated by 200 Å. This result is somewhat surprising; one would have intuitively expected (based on continuum elasticity) the strain modulations to have decayed at that distance (almost two periods) away from their source. Complete decay of the modulations to the resultant average strain would have given a shift of only 8 meV, in contrast to the 21 meV observed. We have also observed similar redshifts in CL spectra of *single* wires produced by overgrowth on *isolated* InGaAs strained layers. Complete relaxation in these cases would have resulted in zero energy shift. Moreover, different shifts are observed due to different strained-layer thicknesses. This is yet another clear indication of quantum confinement, which we will publish elsewhere. To fully understand why the strain modulations penetrate that far, a detailed treatment of the strain distribution in these extreme conditions is required. Such treatment has not yet been carried out, and is beyond the scope of this first report.

Second, almost no broadening of the CL from the SQWR is observed, indicative of the high quality of the crystalline structure. We did observe, however, increased shifts when the electron beam was directed close to the SLS-buffer interface, which we attribute to strain variations in this dislocated region. Third, the CL from the SQWR is as efficient as that from the QWs, though from areal considerations it is expected to be less. This is indicative of the combined effects of increased carrier collection efficiency and the enhanced oscillator strength of the SQWR.

For the PL and PLE measurements, light from a cw dye laser was focused at normal incidence onto the  $(110)$  overgrown facet of the sample using a  $60\times$  microscope objective mounted in the He-flow cryostat. The emitted light was collected from the sample side and analyzed by a 0.25-m double monochromator and cooled photomultiplier. The lowest dashed curves in Figs. 2(a) and 2(b) are the PL spectra. Two PLE spectra are also shown for each QW and each SQWR. The dashed and solid PLE curves were obtained with incident polarization parallel [ $(\bar{1}\bar{1}0)$  direction] and perpendicular [ $(001)$  direction] to the wires, respectively. The PL linewidths of the unstrained QWs are comparable to those measured by CL; however, the linewidths of the SQWRs are much broader because PL also probes the dislocated areas.

The assignments of excitonic transitions in the PLE spectra are marked in Fig. 2(a). The numbers refer to the conduction-band sublevel and the valence-band sublevel, and the letter *H* (*L*) indicates that this is a heavy- (light-) hole subband. These sublevels result from confinement in the  $(110)$  direction, and the observed transitions agree to within 3 meV with the calculated ones. In marked contrast to the unpolarized PLE of a conventional  $(100)$  QW, the  $(110)$  QWs show clear polarization dependence. The light-hole transitions are polarized in

the (001) direction and heavy-hole transitions in the (110) direction. In Fig. 2(b) additional quantum numbers are added to the conduction- and valence-band sublevels to indicate the confinement in the (001) direction. The heavy-hole transitions in the PLE of the SQWR are redshifted  $\sim 17$  meV relative to the corresponding QW transitions, while the light-hole transitions are redshifted by as much as 28 meV. The shifts are almost the same for both SQWRs and for both  $n_{(110)}=1$  and 2 transitions. Optical transition intensities are measured by integrating under the excitonic peaks after background subtraction. Extreme changes are observed in the transition intensities and polarization anisotropy of the SQWRs compared to those of the unstrained QWs. We first note that the light-hole transitions are stronger than the heavy-hole ones, in clear contrast with the unstrained QWs. Second, the light-hole transitions are polarized more than 5:1 perpendicular to the wires [(001) direction] and the  $n_{(110)}=1$  heavy-hole transitions are polarized roughly 3:1 parallel to the wires [(110) direction], whereas the  $n_{(110)}=2$  heavy-hole transition is almost unpolarized.

We evaluate the strain by solving Hook's tensorial equation for the side-grown epitaxial layer. The stress applied by the substrate to the layer is biaxial with unequal components in the (110) and (001) directions. For our system, the displacement in the (110) direction is zero and the displacement in the (001) direction is given by the difference between the GaAs lattice constant and the strained InGaAs lattice constant. With these constraints we find

$$\epsilon_{xx} = \epsilon_{yy} = \frac{\epsilon_{xy}}{2} = \frac{-C_{12}}{C_{11} + C_{12} + 2C_{44}} \epsilon_{zz}. \quad (1)$$

The  $\epsilon_{ij}$  are the components of the strain tensor, the  $C_{ij}$  are the components of the stiffness tensor, and  $\epsilon_{zz}$  is given by  $(a_{\text{SLS}} - a_{\text{GaAs}})/a_{\text{GaAs}}$ . Here  $a_{\text{SLS}}$  is the strained  $\text{In}_x\text{Ga}_{1-x}\text{As}$  lattice constant which is measured by HRXRD.<sup>12</sup> This gives  $\epsilon_{zz} = 0.87\%$ .

To model the structure within the effective-mass approximation, it is necessary to solve eight coupled differential equations<sup>15</sup> which contain both first- and second-order  $\mathbf{k} \cdot \mathbf{p}$  terms<sup>16</sup> and strain terms.<sup>17</sup> Some insight can be gained, however, using the following simplifications: First, the one-dimensional unstrained QW eigenvalues are determined using a conventional method and bulk parameters.<sup>18</sup> From the known energy eigenvalues and effective masses, the discrete effective  $\mathbf{k}$  vectors of the carriers in the confinement direction (110) are determined. The dispersion curves of bulk GaAs for  $\mathbf{k}$  vector parallel to the (110) direction are then calculated, with and without strain, by numerically diagonalizing the  $8 \times 8$  Hamiltonian matrix. The results are depicted in Fig. 3(a).

The lateral band offsets due to the strain can now be determined from the difference between the strained and unstrained dispersion curves for  $k$  vectors which correspond to the QW confined levels. For electrons, con-

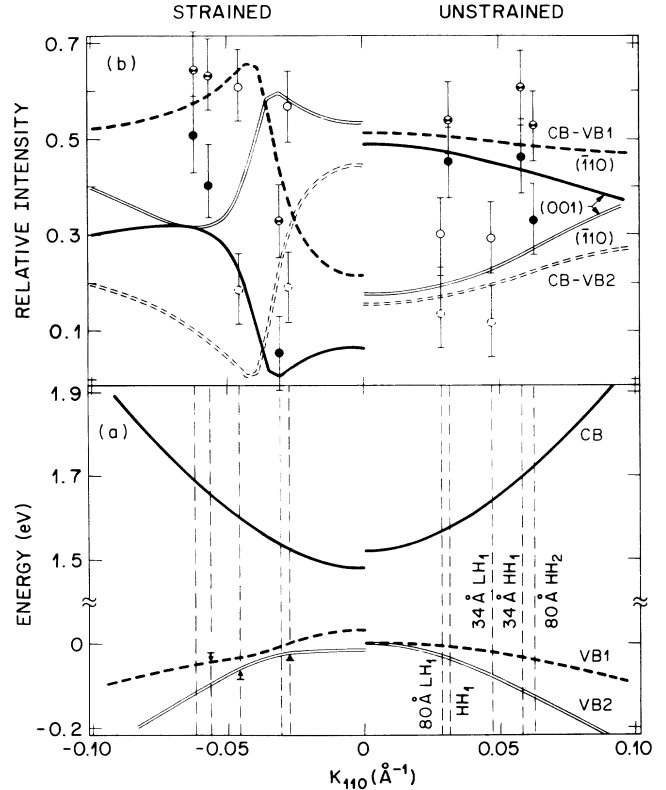


FIG. 3. (a) Dispersion curves and (b) calculated (lines) and measured (circles with error bars) relative optical transition intensities with (left-hand side) and without (right-hand side) strain. The full lines and circles refer to the upper valence band and the hollow ones to the second valence band. Solid lines and circles are for light polarized parallel to (001) and dashed ones are for light polarized parallel to (110).

fining potentials of 30–40 meV are obtained, depending slightly on the specific  $k$  value. For holes the situation is much more complicated. For the relevant range of  $k$ , the offsets are relatively small (up to  $\sim 10$  mV) and they are so strongly dependent on  $k$  that even changes in sign are observed. For the particular  $k$  values corresponding to confinement in the (110) quantum wells, the valence band shifts with strain as indicated by the arrows in Fig. 3(a). The energy difference between the heavy-hole and the light-hole bands shrinks, in agreement with the shifts shown in Fig. 2. Since from Fig. 3(a) we learn that the strain-induced confinement energies in the valence bands are smaller than the excitonic binding energy,<sup>5</sup> they will not be discussed further.

The optical matrix elements for interband transitions are calculated from the eigenfunctions resulting from the diagonalization procedure. The interband optical transition intensities for light polarized in the (001) direction (solid line) and in the (110) direction (dashed line) are shown in Fig. 3(b). Transitions from the uppermost valence band (“heavy hole”) are represented by full lines, whereas transitions from the second valence band are represented by hollow lines. For comparison, the ex-

perimentally measured relative transition intensities are also shown as circles with error bars. The theoretical curve and experimental points exhibit similar trends. We therefore explain the enhancement of the light-hole transitions and the increased polarization anisotropy of the SQWR in Fig. 2(b) in terms of mixing of Bloch wave functions under the particular conditions of strain and confinement in the system. The different behavior of the  $1111_H$  and the  $2121_H$  transitions, however, reflects the different symmetries of the envelope wave functions. This strong indication of the 1D nature of the system has already been observed in wider quantum wires.<sup>5</sup>

The strain-induced confinement in the conduction band can be treated fairly accurately, with the offsets and mass obtained from Fig. 3(a). This is done by solving the 2D effective-mass Schrödinger equation, with the potential structure of Fig. 1(b), by means of a Fourier-analysis model.<sup>4</sup> Periodic boundary conditions are used with the model to take into account the periodic potential in the (001) direction. We find only one quantum number associated with confinement in the lateral (001) direction. This results in two confined eigenstates ( $n_{(110)}=1; n_{(001)}=1$ ) and ( $n_{(110)}=2; n_{(001)}=1$ ) with energies of 62 and 187 meV, respectively, relative to the SQWR conduction-band edge. Subtracting the strain-induced offset of 38 meV and comparing to the 43- and 166-meV confinement energy of the unstrained QW, we calculate redshifts of 19 and 18 meV, respectively. This is in very good agreement with the experimentally observed shifts. A similar result, with only one ( $n_{(110)}=1; n_{(001)}=1$ ) state is found for the  $34\text{-}\text{Å}\times 71\text{-}\text{Å}$  SQWR. Here we have not taken into account elastic relaxation of the strain with distance from the strained layers. This would reduce the amplitude of the potential modulation and increase the dimensions of lateral confinement. For small relaxations the two effects would tend to cancel each other.

In summary, we have fabricated GaAs/GaAlAs quantum wires which exhibit optical properties due to nanometer-scale lateral confinement. The confinement is produced by modulating the in-plane lattice constant of a quantum well grown on an InGaAs/GaAs strained-layer superlattice. The strain-induced band-gap modulation and lateral confinement of carriers manifest themselves in a drastic change of the optical polarization selection rules and a large redshift of the PL and PLE spectra. The experimental observations are in very good agree-

ment with a theoretical model based on the effective-mass approximation and deformation-potential theory. These structures provide a new range for studies of the optical and transport properties of 1D systems.

<sup>1</sup>Y. Arakawa and H. Sakaki, *Appl. Phys. Lett.* **40**, 939 (1982).

<sup>2</sup>M. A. Reed, N. Randall, R. J. Aggarwal, R. J. Matye, T. M. Moore, and A. E. Westel, *Phys. Rev. Lett.* **60**, 538 (1988).

<sup>3</sup>K. Kash, A. Scherer, J. M. Worlock, H. G. Craighead, and M. C. Tamargo, *Appl. Phys. Lett.* **49**, 1043 (1986).

<sup>4</sup>D. Gershoni, H. Temkin, G. Dolan, J. Dunsuir, S. N. G. Chu, and M. B. Panish, *Appl. Phys. Lett.* **53**, 995 (1988).

<sup>5</sup>M. Kohl, D. Heitmann, D. Grambow, and K. Ploog, *Phys. Rev. Lett.* **63**, 2124 (1989).

<sup>6</sup>J. S. Weiner, G. Danan, A. Pinczuk, J. Valladares, L. N. Pfeiffer, and K. West, *Phys. Rev. Lett.* **63**, 1641 (1989).

<sup>7</sup>J. Cibert, P. M. Petroff, G. J. Dolan, S. J. Pearton, A. C. Gossard, and J. H. English, *Appl. Phys. Lett.* **49**, 1275 (1986).

<sup>8</sup>K. Kash, J. M. Worlock, M. D. Sturge, P. Grabbe, J. P. Harbison, A. Scherer and P. S. D. Lin, *Appl. Phys. Lett.* **53**, 782 (1988).

<sup>9</sup>E. Kapon, D. M. Hwang, and R. Bhatt, *Phys. Rev. Lett.* **63**, 430 (1989).

<sup>10</sup>M. Tsuchiya, J. M. Gaines, R. H. Yan, R. J. Simes, P. O. Holtz, L. A. Coldren, and P. M. Petroff, *Phys. Rev. Lett.* **62**, 466 (1989).

<sup>11</sup>H. M. Cox, P. C. Morais, D. M. Hwang, P. Bastos, T. J. Gmitter, L. Naser, J. M. Worlock, E. Yablonovitch, and S. G. Hummel, in *Gallium Arsenide and Related Compounds 1988*, edited by J. Harris, IOP Conference Proceedings No. 96 (Institute of Physics, Bristol and London, 1989), p. 119.

<sup>12</sup>J. M. Vandenberg, D. Gershoni, R. A. Hamm, M. B. Panish, and H. Temkin, *J. Appl. Phys.* **66**, 3635 (1989).

<sup>13</sup>D. Gershoni, J. M. Vandenberg, S. N. G. Chu, H. Temkin, T. Tanbun-Ek, and R. A. Logan, *Phys. Rev. B* **40**, 10017 (1989).

<sup>14</sup>L. N. Pfeiffer, K. W. West, H. L. Stormer, J. Eisenstein, K. W. Baldwin, D. Gershoni, and J. Spector, *Appl. Phys. Lett.* **56**, 1697 (1990).

<sup>15</sup>G. Bastard, *Phys. Rev. B* **25**, 7584 (1982).

<sup>16</sup>E. O. Kane, in *Physics of III-V Compounds, Semiconductors and Semimetals*, edited by R. K. Williardson and A. C. Beer (Academic, New York, 1966), Vol. 1.

<sup>17</sup>G. E. Pikus and G. L. Bir, *Fiz. Tverd. Tela* **1**, 154 (1959) [*Sov. Phys. Solid State* **1**, 136 (1959)].

<sup>18</sup>D. Gershoni, H. Temkin, M. B. Panish, and R. A. Hamm, *Phys. Rev. B* **39**, 5531 (1989).

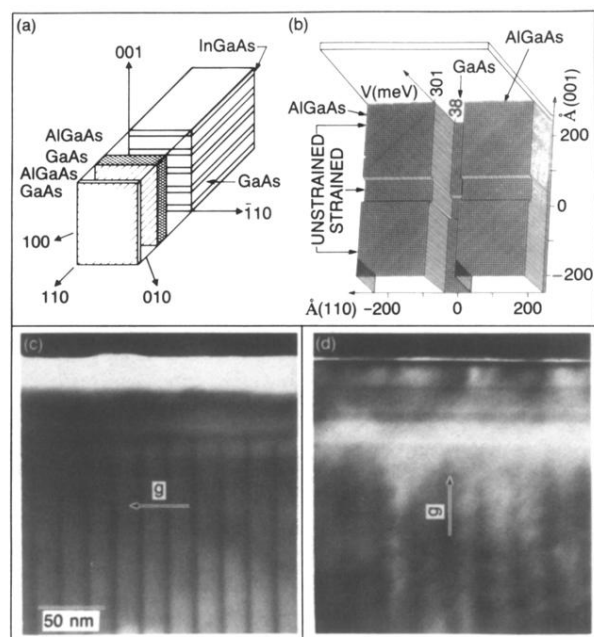


FIG. 1. (a) Schematic of the structure. (b) Calculated conduction-band potential for the  $80\text{-}\text{\AA} \times 71\text{-}\text{\AA}$  strained quantum wire. (c)  $(00\bar{2})$  and (d)  $(\bar{2}\bar{2}0)$  dark-field reflection TEM micrographs of the  $(110)$  side-grown quantum wires.